Evolution of Weak Magnetic Fields in a Turbulent Plasma: A Galaxy Cluster Context

A. Emerick

School of Physics and Astronomy, University of Minnesota, Minneapolis, MN 55455

May 12, 2013

Submitted under the supervision of Dr. Thomas W. Jones to the University Honors Program at the University of Minnesota-Twin Cities in partial fulfillment of the requirements for the degree of Bachelor of Science, *summa cum laude* in Astrophysics.

Abstract

Magnetic fields play an important role in astrophysical objects, in everything from planet formation through large scale structure evolution. The understanding of how these fields evolve and affect the medium in which they are contained has been bolstered through complex computational simulations of both the micro physics involved, and on cosmological scales. I focus on the context of magnetic fields in diffuse plasmas such as that present in the intracluser medium (ICM) of galaxy clusters. In this paper, I examine the evolution of initially weak magnetic fields through solenoidally driven turbulence in a plasma medium. This evolution is expected to be controlled predominantly by the small scale turbulent dynamo until the system reaches equillibrium. The relevant time domain in galaxy clusters, with eddy turnover times on the order of a few to several Myr, corresponds to well before the equillibrium stage. I focus then on the early magnetic field evolution and turbulent amplification under three initial magnetic field conditions utilizing an ideal, isothermal MHD code. I examine the detailed time and power spectra evolution of both the kinetic and magnetic energies, and compare to what would be expected in the small scale dynamo picture. In addition, I examine the prospects of distinguishing initial magnetic field structures within the ICM.

Contents

List of Tables

List of Figures

1 Introduction

Galaxy clusters are the largest virial objects in the universe, containing 10^2-10^3 galaxies, with total masses around 10^{14}-10^{15} $M_\odot$. Roughly 10% of the total cluster mass is baryonic matter, as most of the cluster mass lies in the dark matter halo. Most of this baryonic matter resides within the hot diffuse plasma interspersed throughout the space between constituent galaxies in the cluster, called the intracluster medium (ICM). The ICM, heated to temperatures on the order of 10^7 and 10^8 K, is marked by strong thermal X-ray emission. In addition, many clusters exhibit a diffuse, non-thermal radiation component produced by the synchrotron emission of charged particles that are accelerated through various processes in the ICM. This often takes the form of radio halos, or Mpc scale sources of diffuse emission that are distinct from any point sources of radio emission (e.g. radio galaxies). Observations of these radio halos in the Coma cluster (and others) have established the presence of a magnetic field ranging from a few μG at the cluster center to $\sim$0.1 μG at cluster outskirts (Brunetti et al., 2001). Faraday Rotation Measurements have established the presence of fields in clusters with significant variation in strength and coherence, $\sim$0.1-10 μG and $\sim$1-10^2 kpc, depending upon individual cluster properties; see Carilli & Taylor (2002) for references to recent measurements. It remains an important scientific question as to how these fields, once established at some scale, are amplified to the μG levels indicated by observation.

Magnetic fields are ubiquitous throughout the universe and play an essential role in a host of astrophysical objects. On Earth, for example, they exist on $\sim$0.5G levels, shielding its atmosphere from cosmic radiation. They are produced from the convection of plasma in stars, like our sun, and are responsible for sunspots and solar flares, where the field strength can reach up to 10^3G. Magnetic fields play important roles in planet and star formation, and are present within the interstellar medium of galaxies. Only in the past few decades have studies been made to attempt to observe and understand even larger scale magnetic fields, such as those found in the ICM. Magnetic fields play an important role in clusters, influencing the viscosity, resistivity, and thermal conductivity of the ICM. In addition, fields act to accelerate charged particles through first and second order Fermi acceleration, sustaining the observed radio emission in clusters. Also, they contribute to the propagation of ultra-high energy cosmic rays. Takami et al. (2012) contains a discussion of the effects of galactic and extragalactic magnetic fields on observations. Cosmological simulations of clusters provide a great insight into their evolution, serving to test of our understanding of cluster phenomenology. In order to properly model and understand these systems, we must have a firm grasp of the micro-physics, especially relating to MHD turbulence and the evolution of magnetic fields; see (Brandenburg & Subramanian, 2005) for a recent review. Much work has been done recently on the evolution of initially uniform magnetic fields, with emphasis on the late evolution of these systems, where the kinetic and magnetic energy densities reach an equilibrium state.

This is more applicable to stronger magnetic fields in the intergalactic medium (IGM) (Cho et al., 2002), relaxed systems, or systems old enough to have experienced many eddy turnovers on the largest scales. In the context of clusters, however, the relevant timescales are such that the system could very well be far from this equilibrium state; although the eddy turnover timescales are smaller than the relevant merger timescale of clusters, they are only so by a factor of few.

The ICM is a tumultuous medium, driven on multiple scales by various astrophysical processes including cluster mergers, accretion, active galactic nuclei, galactic winds, and various plasma instabilities. Shocks generated from these phenomena, along with large scale shear from the relative motions of cluster substructures, provide a source of turbulence in the ICM. The origin of these fields in clusters is a topic of current research; Ryu et al. (2012) provides a recent review of magnetic field formation in large scale structures of the universe. For clusters specifically, fields have been posed to originate prior to recombination, in ejection from galaxies (mainly AGN), and/or the establishment of seed fields through the Biermann battery mechanism. Although field origin is an unanswered question, we know that, since the magnetic diffusion timescale for clusters is much longer than the age of the universe, once established, magnetic fields will remain in clusters for a long time, unless disrupted by processes such as magnetic reconnection (Carilli & Taylor, 2002). Therefore, once established by some means, they will be highly subject to the "weather" of the ICM; it is the interaction between the ICM and these possible seed magnetic fields that is thought to generate the observed μG fields.

Turbulence has been shown to effectively amplify weak magnetic fields through the stretching and folding of magnetic fields lines. This amplification process is referred to as the turbulence dynamo, or the small-scale dynamo. A second growth mechanism is referred to as the large-scale dynamo, where fields coherent on the scale of the size of the given astrophysical object are amplified by a mixture of effects, such as turbulence, object rotation, velocity shear, and field helicity. The former is more efficient, and thus significant, in a cluster context, and is the focus of this paper. Research in this area has seen gradual progression over the past half-century, as models, computational techniques, and computing power have improved substantially. Computing power is the primary limiting factor preventing the simulation of the entire situation of field evolution in clusters (i.e. cosmological scale). This endeavor is prohibited by the necessity of detailed resolution on the system scale (L), down to the turbulence driving scale (l_0), to the viscous dissipation scale (l_ν), and to the magnetic dissipation scale (l_η) — this comprises a very large dynamic range, as $L \gg l_0 \gg l_\nu \gg l_\eta$. In an ideal MHD environment, the viscous dissipation and magnetic dissipation scales will be comparable ($l_\nu \sim l_\eta$), as each is the result of numerical effects on the order of the simulation grid size. Even though we are restricted to focusing on only part, not all, of these three ranges in a given simulation, it is important regardless to focus efforts towards understanding the detailed microphysics of field growth in turbulent media, in addition to cosmological scale studies, in

order to better piece together what is happening in the larger context of the ICM.

An interesting avenue towards exploring how and where fields arise first in galaxy clusters is attempting to identify what, if any, signatures from the initial magnetic field structure remain presently in the ICM. It is expected that after a long enough time scale, many eddy turnover times, the final equilibrium state of the magnetic field is independent of its initial structure. At some point during the evolution of the cluster and the ICM, the turbulent motions erase any details required to probe the initial field structure. It is an important question as to exactly when in the course of cluster evolution is this point reached, as it may be possible some signatures of the initial field structure remain in young or recently merged galaxy clusters. In this context, we examine the early evolution of the magnetic field in attempts to identify how long signatures of the initial structure persist in the evolving medium.

We concern ourselves here with the evolution of an already present small-scale weak magnetic fields, and their development via the small-scale turbulent dynamo. We examine the interplay between turbulence and a magnetic field fixed such that the overall mean field is zero - but with some random coherence on small scales - under a variety of initial conditions. We compare these results at various resolutions to the evolution of an initial overall uniform mean field. We place special emphasis on the early evolution of the system, concerned with the beginning phases of field amplification. In this paper, we utilize an updated isothermal, ideal MHD code developed in Kim et al. (1999). We discuss our code and numerical methods in Sec. 2, and describe the set up of our simulations in Sec. 3. We present the results of our simulations, examining the time and spectral evolution of the magnetic and kinetic energies in Sec. 4, and provide a discussion of their implications in Sec. 5. We conclude in Sec. 6.

2 Numerical Methods

We utilize a numerical scheme that constructs and solves the ideal MHD equations which, by definition, ignore the explicit inclusion of electrical resistivity and viscosity. In addition, our scheme is isothermal, ignoring thermal conductivity and fixing a constant temperature throughout the plasma medium. We solve the following equations:

$$\frac{\partial \rho}{\partial t} + \nabla \cdot (\rho \vec{u}) = 0, \tag{1}$$

$$\frac{\partial \vec{u}}{\partial t} + \vec{u} \cdot \nabla \vec{u} + \frac{1}{\rho} \nabla \left(a \rho^2 \right) - \frac{1}{\rho} \left(\nabla \times \vec{B} \right) \times \vec{B} = 0, \tag{2}$$

$$\frac{\partial \vec{B}}{\partial t} - \nabla \times \left(\vec{u} \times \vec{B} \right) = 0, \tag{3}$$

$$\nabla \cdot \vec{B} = 0. \tag{4}$$

The units are assigned to remove any factors of 4π, through the inclusion of $1/(4\pi)^{1/2}$ in $\vec{B}$. a is the isothermal sound speed, set to unity, while the rest of the terms have their standard meanings. The initial mean plasma density, ρ, is also set to unity, so that, for the isothermal equation of state, the initial mean gas pressure is also unity, as P_g=a^2=1.

The code is an extension upon a one-dimensional conservative model (Ryu & Jones, 1995) that solves the above ideal MHD equations in an explicit finite-difference scheme called the total variation diminishing (TVD) scheme (Harten, 1983), based upon a second-order extension of the Roe-type upwind scheme (Roe, 1981). The basic one-dimensional case is carried to multiple dimensions (Ryu et al., 1995) through a Strang-type operator splitting (Strang, 1968). In this extension, a constrained transport method (Evans & Hawley, 1988) is used to describe the magnetic field at grid interfaces, with advective fluxes defined at grid edges; these are used in the staggered mesh technique to constrain the magnetic field transport and guarantee Eq. (4) exactly (Ryu et al., 1998). The MHD equations (1)-(3) are rewritten in a Jacobian matrix, and the left and right eigenvectors are found, with seven eigenvalues. In the TVD scheme, the physical quantities of each grid cell are placed at the cell centers, while fluxes are calculated at the boundaries between adjacent cells. We employ periodic boundary conditions when calculating the flux at the edges of the simulation box. The extension of the Roe linearization scheme mentioned above is then constructed to compute the relevant physical quantities for each cell. An explicit and detailed explanation of the construction of our numerical scheme, including detailed tests of its validity, can be found in Ryu et al. (1995).

An ideal MHD simulation does not contain an explicit diffusive term, -$\eta\nabla^2\vec{B}$, in Eq. (3), the induction equation. However, numerical dissipation is a present and unavoidable consequence of finite grid resolution. In the isothermal case, thermal conductivity is eliminated, preventing heat loss; thus the numerical dissipation acts like a modified form of viscosity and resistivity which is a function of the grid size. The significance of dissipation, and its relationship to simulation resolution, can be identified by observing the decay of linear Alfvén waves. This test was conducted in Kim et al. (1999) constructing a simulation where ρ_o=1, $\delta v_z = v_{amp}\sin(k_x x + k_y y)$, $\vec{B} = 1 \cdot \hat{x}$, and all other quantities are set to zero. This was performed in a square periodic box of size L, for L=1, with $2^n \times 2^n$ cells, where n = 3,4,5,6,7. $k_x = k_y = 2\pi/L$ was set. The numerical Reynolds numbers were estimated as a function of the number of cells, given in Fig. 1, giving the relation that R$\propto n_{cell}^2$. This indicates that the code is second-order accurate, with about 50% smaller numerical dissipation than the related adiabatic MHD code. As the grid resolution approaches unity, the magnetic Reynolds number also approaches unity.

Since the origin of our resistivity and viscosity is numerical, the resistive dissipation scale (l_ν)is on the order of the grid resolution. It is important to note that the magnetic Prandtl number, defined as $P_{r,m}$= R_m/R_e=ν/η, is $P_{r,m} \sim 1$ in our simulations, since $l_\nu \sim l_\eta$ and therefore $\nu \sim \eta$. It is possible for

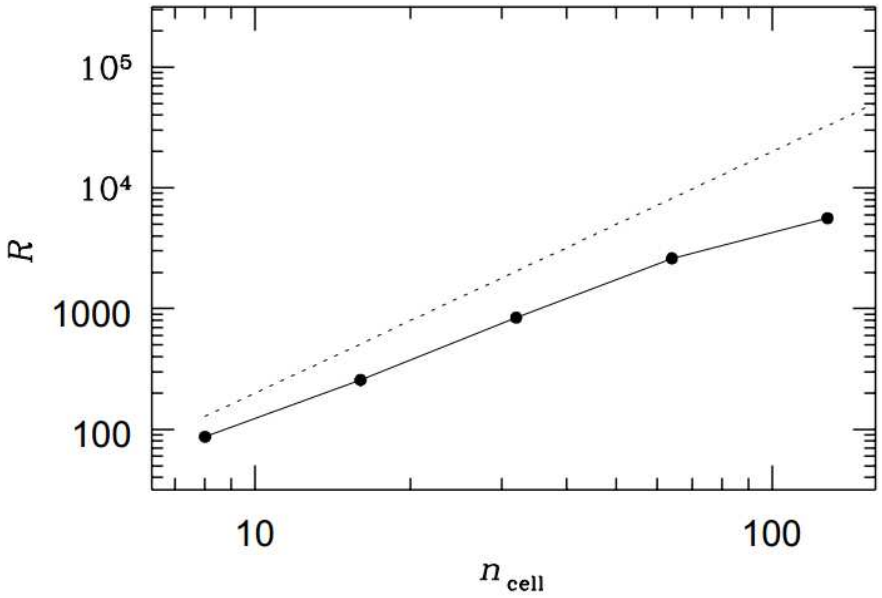

Figure 1: The magnetic Reynolds number calculated as a test of the decay of Alvén waves by numerical dissipation. The magnetic Reynolds number scales roughly as n^2. This plot has been taken from Kim et al. (1999)

the hot, diffuse ICM to have Prandtl numbers much greater than unity, as $P_{r,m} \propto T^4/n$, where n is the number density of the plasma. However, simulating these cases is a challenging process, as one runs into the issue discussed previously of having to resolve the system over a large dynamic range of scales(see Schekochihin et al. (2004)). Modeling these systems at a high, converged resolution is not yet possible. For this reason, we choose to follow many previous works remaining with $P_{r,m} \sim 1$. Ultimately, however, a complete study would require exploration into the $P_{r,m} \gg 1$ regime.

3 Simulations

In each simulation, we set initial properties of the turbulent flow that is acting on the system. In each case, the flow properties remain the same, while we vary the initial conditions on the magnetic field. The constructed turbulent flow is restricted to a purely solenoidal driving component, with no driving in the compressional mode. In reality, turbulence in the cluster context and in the context of any astrophysical object will be some combination of solenoidal and compressional driving. In the context of galaxy clusters, compressional amplification of fields is associated with the effects of shocks developed within the ICM through large scale structure formation, and processes such as cluster mergers. Compressional effects, however, are more relevant in answering the question of how galaxy cluster magnetic fields are established in the ICM in the first place, on the nanogause level; see (Ryu et al., 2003; Medvedev et al., 2006; Kang et al., 2007; Skillman et al., 2008) for discussion of shocks in clusters. Once well established,

the amplification of magnetic fields from vortical motions in the medium to the observed microgause levels will be produced primarily from solenoidal motions; this is our focus.

The simulation box is set with dimensions L_o=L_x=L_y=L_z=10. Since the sound speed is set unity, and the time units are defined to be the sound crossing time of one length unit, the box sound crossing time is 10. The velocity field is driven impulsively every 0.1 time units separated into solenoidal ($\nabla \cdot \delta\vec{u}$=0) and compressional ($\nabla \times \delta\vec{u}$=0) components with a Helmholtz decomposition; again, we concentrate on purely solenoidal driving. The energy injection contains random fluctuations, determined by a set of Fourier modes randomized with random phases and amplitudes. The fluctuations obey a power law with respect to wave number according to $k^4 e^{-(k/k_{peak})^2}$, and are scaled so that the average energy injection rate per unit volume is maintained at dE_K/dt=0.016. The fluctuation injection is cut off at wavelengths 1/10 the box size. k_{peak} is fixed such that the maximum of the injected fluctuations occurs at $2k_o$, where k_o=$2\pi/L_o$; this is referred to as the driving scale. This corresponds to L_d=$L_o/2$; the amplitude of these injections is tuned such that the RMS turbulent velocity is $u_{RMS} \sim 0.5$, corresponding to an eddy turnover time of roughly t_d=L_d/u_{RMS}=10.

We construct several simulations, varying input parameters pertaining to the initial magnetic field structure at various resolutions; these are presented in Table 1. In our examination, we observe how the magnetic field grows over very early times, well before the system reaches equilibrium. Currently, we have performed 128^3, 256^3, and 512^3 resolution simulations for each initial field case, with the latter used as the focus of this paper. We focus our analysis on three simulations, each beginning with the same total magnetic field energy E_B=10^{-4}. The first contains an initial uniform field across the entire box, with magnetic energy concentrated solely in B_x, with no initial field structures. Uniform field simulations have been well studied previously, and is used here as a comparison between our k4-8 and k8-16 simulations. The former, k4-8, contains a zero mean magnetic field contained within $4<k/k_o<8$; in other words, the initial field direction is randomized in such a way that the total net magnetic field across the simulation box is zero. The later, k8-16, contains a zero mean magnetic field contained within scales twice as small, $8<k/k_o<16$. In these two simulations, the magnetic field energy spectra within these regions is fixed as flat. For comparison of $E_K(k)$, see Sec. 4.2, we also conduct a hydrodynamical simulation using the same parameters, yet with no initial magnetic field.

Fig. 2 shows the initial magnetic field spectra for k4-8 and k8-16 in comparison to the velocity field spectrum immediately after the first energy injection. Fig. 3 gives a rendering of the magnetic field lines in the 512^3 resolution simulation for both initial field mode ranges. This 3D rendering traces the field lines for a specified length in a 75x75x1 grid of sample points. Color here denotes the direction of a given field line, with the field line traced from its start (blue) to its end (white). For long field lines the color may alternate several times, providing an easy way to identify the direction. A comparison between the

Run Name	Highest Resolution	Initial Field Type	E_B at t=0	k_{min}	k_{max}	k_{max} fluctuation
Uniform	512^3	$B_x=10^{-2}$ $B_y=B_z=0$	10^{-4}	-	-	-
k4-8	512^3	Zero mean B-field	10^{-4}	4	8	10
k8-16	512^3	Zero mean B-field	10^{-4}	8	16	10
Hydro	512^3	None	0	-	-	-

Table 1: This table gives the relevant initial conditions set to the magnetic field for the four simulations discussed in this paper. Each simulation was run first at 128^3 and 256^3 resolution, with the highest, and focus of this paper, at 512^3.

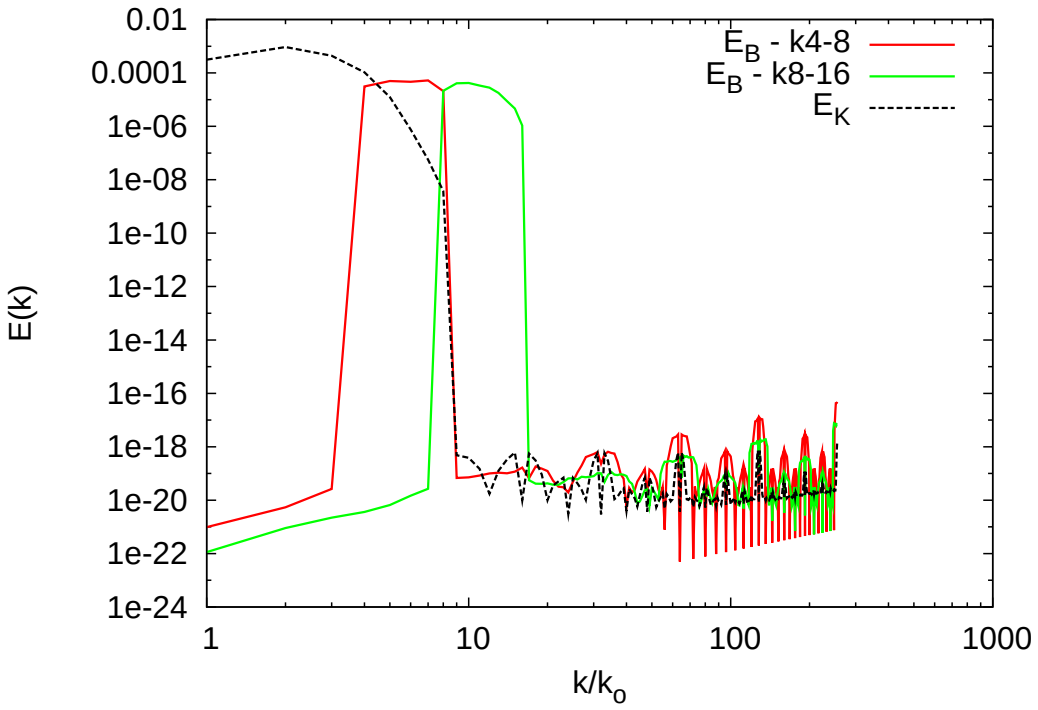

Figure 2: The power spectra of the velocity field just after the initial energy injection, and power spectra of the initial magnetic fields at 512^3 for the k4-8 and k8-16 simulations. The velocity field here is taken from the hydro simulation, but is the same for each case.

two initial field structures in Fig. 3 makes the differences between these two simulations apparent. Fig. 4 shows the initial velocity field structure, where, again, color denotes direction of field lines.

The small scale turbulent dynamo is expected to be the dominant source of growth of the magnetic field once turbulence is established on the smallest scales. It operates through the stretching and twisting of magnetic field lines, which is especially relevant when the magnetic field lines are frozen into the plasma, as is the case in our ideal MHD simulations. The dynamo first operates in an exponential growth phase once turbulence is established, causing significant growth on small scales that gradually feeds upward. During this phase, the magnetic field energy grows as $E_B \propto \exp(t/t_{eddy})$, and lasts until the magnetic fields establish a significant Lorentz force and begins backreacting on the kinetic flow. During the backreaction phase, the growth is linear with time ($E_B \propto t/t_{eddy}$). Eventually, the magnetic

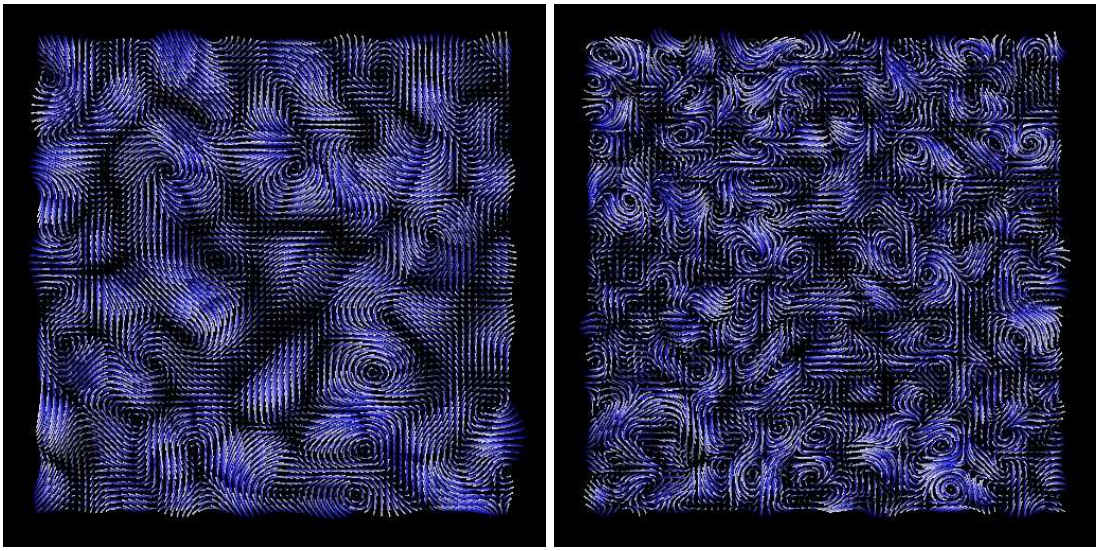

Figure 3: A rendering of the initial magnetic field structures comparing the initial conditions for the two different magnetic field mode ranges used, k4-8 (left) and k8-16 (right). Shown is a 75x75x1 grid of field test points, with field lines drawn to a specified length. The color signifies direction; each field point begins with a blue section then changes slowly to white traveling along the field line.

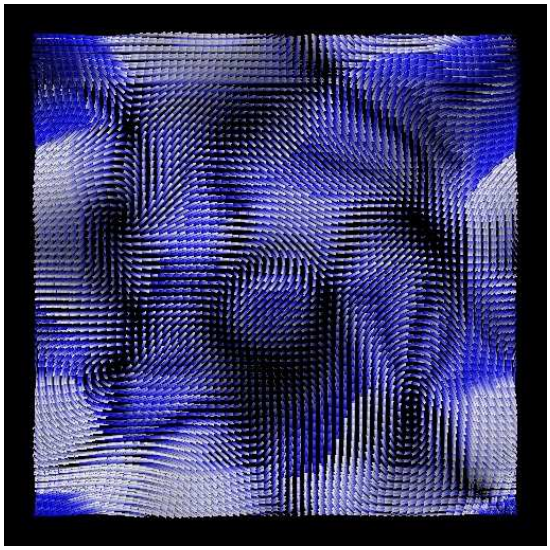

Figure 4: Shown is a rendering of the velocity field structure just after t=0, when kinetic energy is injected into the medium. The rendering contains a 75x75x1 grid of field test points, with color signifying direction along the field lines, from blue to white.

field will saturate, and will reach an equilibrium state (with fluctuations) along with E_K (Ryu et al., 2008). We take the lower resolution simulations out to large timescales to confirm the presence of these three stages in each initial field case. Fig. 5 shows the kinetic energy (dashed) and magnetic energy (solid) growth for the uniform field (blue), k4-8 (red), and k8-16 (green) simulations at 256^3 resolution. Although there is significant difference in rate of change for the magnetic and kinetic energies in each case, this plot clearly shows the exponential growth, linear growth, and saturation phases from the small

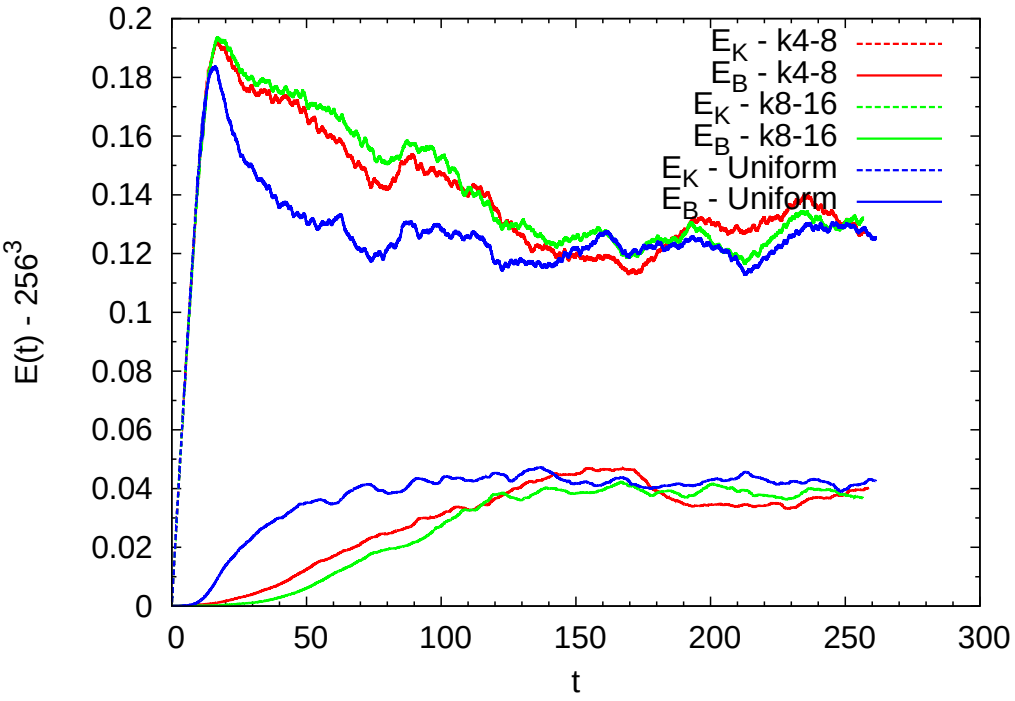

Figure 5: Shown is the energy evolution of the magnetic field (E_B, solid) and velocity field (E_K, dashed) for the uniform field (blue), k4-8 (red), and k8-16 (green) simulations at 256^3 resolution.

scale dynamo. We concern ourselves with the very early stages of the magnetic field growth, primarily how the magnetic field grows before and during the exponential growth phase. We restrict ourselves to t<20 in the 512^3 resolution simulations, allowing a high time resolution on the order of the energy injection rate (0.1 time units).

4 Results

The below provides an analysis of our results in three sections. The first, Sec. 4.1 examines the energy evolution of the system as a function of time in comparison to the expected small scale turbulent dynamo picture. This analysis is further deepened with an examination of the power spectra in Sec. 4.2. We conclude our results in Sec. 4.3 with a brief, qualitative discussion of the relation between numerical dissipation in ideal, isothermal MHD to physical magnetic dissipation.

4.1 Energy Evolution

We report on the evolution of the magnetic and velocity field (in terms of magnetic and kinetic energies) in the three initial magnetic field cases discussed in Sec. 3, referred to as k4-8, k8-16, and uniform field. The time evolution of the magnetic and kinetic energies in these cases provides an immediate insight

into the differences between the evolution of these systems. It is apparent that the growth rate of the magnetic field energy differs significantly depending upon the initial scales of the magnetic fields, as shown in Fig. 6. As given by the small scale dynamo model, the turbulence, once established, causes the magnetic field to grow exponentially with $E_B \propto \exp(t/t_d)$ (ignoring constant factors), where the eddy turnover time is roughly 10 time units in our simulations (Ryu et al., 2008). However, prior to this, the amplification of the magnetic field is not described well.

The systems take some time to fully establish kinematic turbulence, resulting in a delay before the small scale dynamo turns on and becomes the dominant effect. As described in Sec. 4.2, prior to the onset of turbulence, the growth of the magnetic field is dominant on scales near the driving scale for each simulation prior to t=5. In the initial growth of E_B, the simulations are indistinguishable until about t=3, when turbulence in the systems becomes significant and begin to engage the small scale dynamo action. Once the dynamo engages, growth is most significant on the smallest scales, near the dissipation scale, and the time evolution of E_B begins to diverge for each simulation. By around t=5, each simulation has entered the initial exponential growth phase. However, the initial conditions of these simulations dramatically affect the rate of growth during the exponential phase.

In the uniform case, the turbulence more readily amplifies the magnetic field energy, quickly growing to $\approx 5 \cdot 10^{-3}$ by the onset of the linear growth phase around t/t_o=1.3. This growth can be described well by an exponential fit where $E_B \propto \exp(4.2t/t_o)$ for $0.4<t/t_o<1.2$, where t_o is the characteristic eddy turnover time, 10 time units. As magnetic backreaction becomes significant, the exponential growth tapers off from about t=12 to t=13 to a linear growth where $E_B \propto 2.5 \cdot 10^{-2} t/t_o$. It is apparent that the initial field conditions for k4-8 and k8-16 suppress the dynamo relative to the uniform field evolution. Not only this, but the character of the exponential growth in each is inherently different than the model prescribes. For k4-8, there are two distinct exponential growth regions, one during $0.5<t/t_o<0.8$ and the other immediately following at $0.8<t/t_o<1.8$, where $E_B \propto \exp(3.2t/t_o)$ and $\exp(2.0t/t_o)$ respectively. The suppression of the small scale dynamo during this time delays the onset of the linear growth phase until around t=20, where the magnetic field energy here is comparable to the energy in the uniform case during its transition to the linear phase around t/t_o=1.2. The k8-16 simulation proves even more interesting, as two similar exponential growth regions at $0.5<t/t_o<0.8$ and $t/t_o>1.6$, where $E_B \propto \exp(2.1t/t_o)$ and $E_B \propto \exp(2.2t/t_o)$ respectively, are separated by 8 time units by a dip in the growth rate. Whatever effect leading to the suppression of the k4-8 and k8-16 growth rates seems to be temporarily enhanced in this region. Like the k4-8 case, the linear growth phase is delayed to past the maximum time of these simulations. However, the growth of k8-16 is seen to taper off from an exponential just before t=20, so the delay is likely only by a few more time units.

As the time evolution depicts, the small scale turbulent dynamo may be an inadequate model for

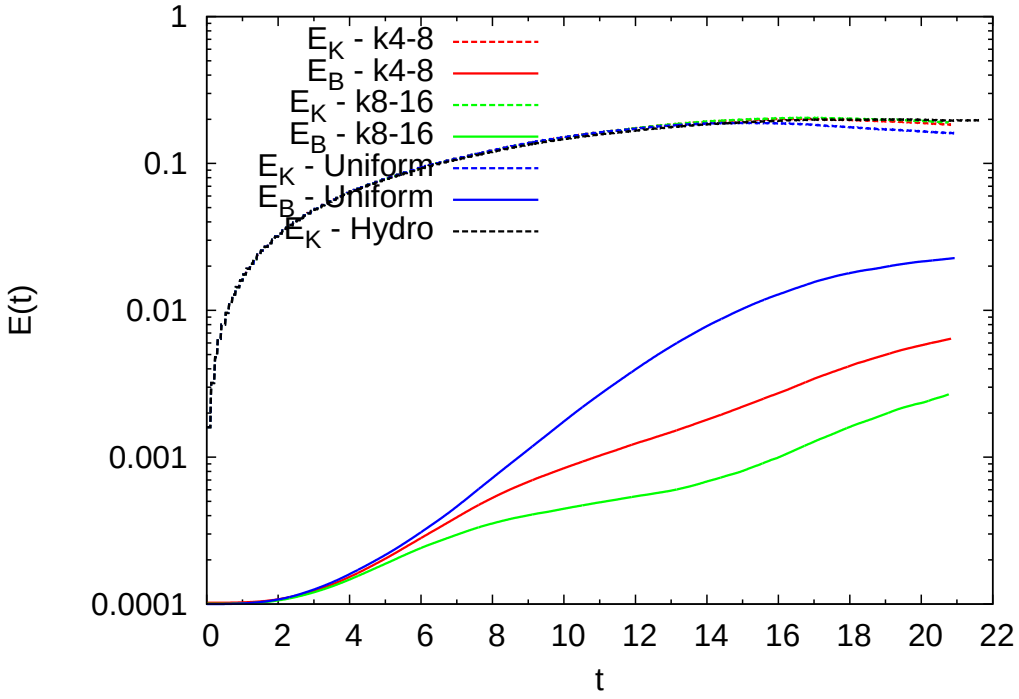

Figure 6: Shown is a comparison between the energy evolution of the magnetic energy (solid) and kinetic energy (dashed) for the three initial field configurations, k4-8 (red), k8-16 (green), and the uniform field (blue), and the hydro case (black).

more complex, non-uniform initial field conditions. It is likely that there are multiple competing effects governing the evolution of these systems. Insight into the departure from this model in these cases is given when considering the power spectra of the kinetic and magnetic energies in Sec. 4.2.

As demonstrated in the low resolution evolution in Fig. 5, the magnetic field energy will eventually saturate to the same level (with fluctuations) regardless of the initial field structure. The saturation process is not of concern in this paper. The kinetic energy here grows quickly in the same fashion for all three simulations to a peak, after which the kinetic energy decreases to an equilibrium state as it feeds the growth of the magnetic field to saturation. The time the systems take to reach this peak corresponds to the large scale eddy turnover time, and is roughly at t=15,16, and 17 for the uniform field, k4-8, and k8-16 cases respectively. The evolution of E_K is similar to the hydro case until the simulations are well into the exponential growth phases, when the magnetic field energy becomes relevant. The hydro case exhibits no peak, and saturates by t=17, while the other three simulations drop below this energy level after their respective peaks. The differences across the three simulations here can be attributed to the differences in the magnetic field growth rate and magnitude; this is seen namely in a delay in the peak of the kinetic energy.

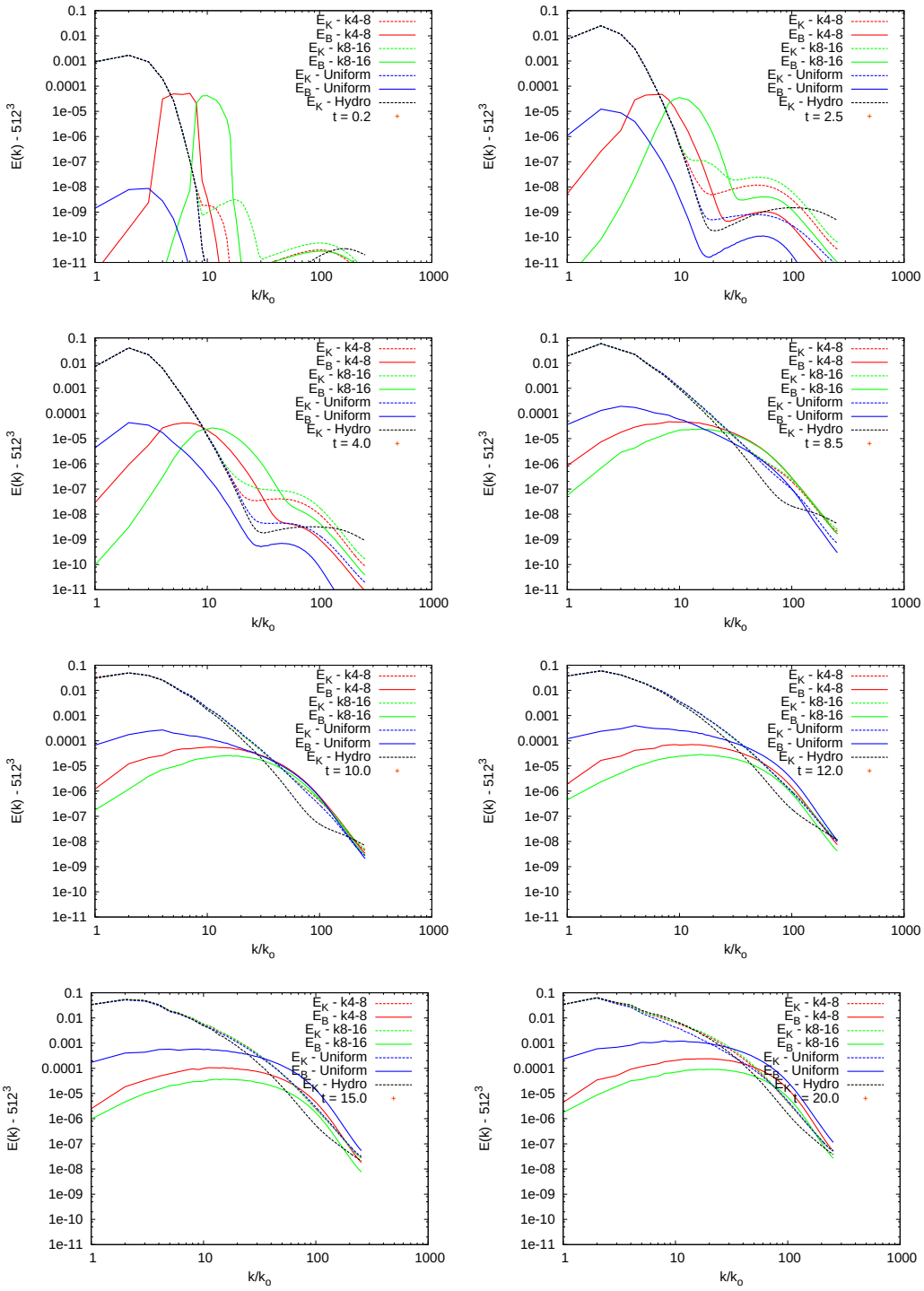

Figure 7: Snapshots of the magnetic (E_B, solid) and kinetic (E_K, dashed) energy spectra at t=0.2, 2.5, 4.0, 8.5, 10.0, 12.0, 15.0, and 20.0. Each plot compares the magnetic energy and kinetic energy spectra between the uniform field (blue), k4-8 (red), and k8-16 (green) simulations each of 512^3 resolution. Included also for comparison purposes is the hydrodynamical simulation (black) with no magnetic fields.

4.2 Energy Cascade: Power Spectra

Fig. 7 gives a comparison between the spectra of each simulation run for $E_B(k)$ and $E_K(k)$ at select times, t=0.2, 2.5, 4.0, 8.5, 10.0, 12.0, 15.0, and 20.0. First, we examine the magnetic field and velocity

field for the k4-8 and k8-16 cases in terms of their power spectra as they evolve through time. These are compared to the initial uniform magnetic field case. Fig. 2 gives the initial spectra for the simulations (only one velocity field is shown here, as the initial field is identical for all three magnetic field cases).

The impact of the various initial field conditions on the evolution of these systems has immediate consequences on the kinetic and magnetic energy spectra from the very start of the simulation. For comparison here, we have included the kinetic energy spectra of the hyrdodynamical case (black, dashed). We will begin with a discussion of the effects on the kinetic energy of each system; first we will focus on the differences between the hydrodynamical case and the three magnetic field systems in general, then discuss the differences between each MHD simulation. The growth of E_K across all simulations is similar on large scales (k/k_o <10), while the smallest scales show immediate differences. The kinetic energy evolution near the driving scale for the MHD simulations begins to diverge significantly from the hydrodynamical case around t=6.0. However, between the three simulations with initial magnetic fields, E_K remains similar for k/k_o <10 through t=20.0. In the initial growth on small scales, it is immediately apparent that the presence of a magnetic field suppresses the kinetic energy on the smallest scales relative to the hydrodynamical case, yet is able to amplify E_K in the middle of the spectrum (more so for the k4-8 and k8-16 simulations than the uniform magnetic field simulation). This explains the slightly enhanced growth rate of $E_K(t)$ for the MHD simulations compared to the hydro simulation. Once the small scale turbulent dynamo turns on for each of the three MHD simulations, a process that begins around t=4.0, E_K begins to diverge significantly from the hydrodynamical case. While E_K in the MHD simulations remains below the hydro energy on the smallest scales until around t=12.0, it is quickly raised above the hydro E_K for all k/k_o >8. Through this time then, the magnetic field serves to amplify the turbulence, especially for mid-range k. However, once the linear growth phase of the small scale dynamo is underway (which occurs for the uniform field around t=12.0), E_K begins to drop below the hydro case for 2<k/k_o <12. This is really only seen for the uniform field, as it is the only one of the three simulations well into the linear growth phase by t=20.0; however, the beginning of this can be seen at t=20.0 (barely) around k/k_o=7. By the end of our simulations, at t=20.0, the kinetic energy takes a Kolmogorov-like form, $E_K(k) \propto k^{-5/3}$, for 2<k/k_o <50 in the hyrdo case. The other MHD simulations reach Kolmogorov-like spectra as well, but only for when magnetic backreaction is still negligible, as is roughly the case for k4-8 by t=20.0, and is the case for k8-16 by t=20.0.

The differences in initial E_K evolution occur on small scales, directly related to the initial magnetic field location. The presence of the magnetic field localized to k4-8 or k8-16 causes enhanced E_K growth at scales just smaller (k/k_o ∼10 for k4-8, and k/k_o ∼11 for k8-16) than the initial field. It appears that the Lorentz force ($\vec{J} \times \vec{B}$) pushes around the plasma near these scales. This has a further effect on smaller scales, as E_K is roughly two orders of magnitude larger at t∼1 in the k4-8 and k8-16 simulations

at k/k$_o$ >10 compared to the uniform case, with k8-16 containing more power on small scales than k4-8. The initial bumps in E_K for k4-8 and k8-16 smooth out by t=1.6 and t=3.0 respectively. As time increases, the kinetic energy in each simulation becomes gradually more similar, eventually becoming almost identical on all scales by t=10. After t=10, the spectra remains roughly uniform until t=15, when a slight enhancement of E_K appears for k4-8 and k8-16 relative to the uniform case for $3 \lesssim$k/k$_o$ $\lesssim 15$. The size of this enhancement grows towards t=20, and is, at its largest, a factor of $\sim$2 greater than in the uniform case, for both k4-8 and k8-16.

The evolution of the magnetic field energy spectra is inherently more complex than the kinetic energy spectra. The evolution of E_B(k) here is described commonly by the small scale turbulent dynamo, where field growth originates on scales much smaller than the energy injection scale (k$_o$) and proceeds through an inverse cascade towards the driving scale. In this picture, field growth is most significant on scales where the turbulence most effectively stretches and twists the magnetic field lines, resulting in a local maximum in the magnetic field spectra at small scales; the scale at which this occurs is expected to be dependent upon both the initial field conditions and the properties of the velocity field (Cho & Yoo, 2012). Recalling the discussion in Sec. 4.1, the evolution begins with an exponential phase once turbulence is established, and subsequently enters a linear growth phase once magnetic back-reaction becomes significant. As seen above, the uniform field case follows this model well, beginning with a consistently exponential phase around t=5 followed by a linear phase around t=15. The other two simulation cases showed a departure from this model in both the nature of the exponential phase, and the time of the onset of the linear growth phase. See Fig. 6.

Second, we examine the uniform field E_B spectra as a baseline for comparison to the other cases. Growth begins immediately and dramatically near the driving scale of the simulation. There is an immediate jump within the first few driving times in the field energy in k/k$_o \leq 10$, peaking at k/k$_o$=2. From here, the spectrum maintains a fixed shape, with the entire spectrum growing in unison as the growth rate decreases towards the driving scale and slowly increases towards the smallest scales. By the time the small scale turbulent dynamo starts to engage, around t=4.0, the spectrum is still peaked about k/k$_o$=2, with a steep ($\sim k^{-3.5}$) fall off to k/k$_o$=12, and a local maximum on small scales at k/k$_o$=50. At this point, growth on the smallest scales becomes significant, beginning the inverse cascade. During this time, the slope from the k=2 peak softens, and the spectrum becomes smooth down to the smallest scale. By t=8, the magnetic field energy begins to overtake the kinetic energy on small scales, specifically near k/k$_o$=60. The field continues to grow and is entirely above the kinetic energy for k/k$_o \geq$30. During this time, the magnetic back reaction becomes significant, and the magnetic field enters the linear growth phase. From here through the end of the simulation, the magnetic field grows slowly over the entire spectrum. By t=20, the magnetic energy spectrum is almost flat for k/k$_o \leq$30, aside from a slight

downturn near the driving scale. Above k/k_o=30, the spectrum is very steep and goes roughly as k^{-5}.

Comparing the growth of the k4-8 and k8-16 cases against the uniform field shows immediate differences between the two from the start of the simulations. Even though the growth in E(t) shown in Fig. 6 is degenerate for the three simulations for the first few time units, the initial field structures create obvious differences in growth on both the largest and smallest scales. The field structure apparently suppresses large scale growth relative to the uniform case significantly, as growth is slow on scales larger than the location of the initial field structure; this suppression is more pronounced in the k8-16 case. The spectrum from the driving scale down to the initial field structure is steeper there as well. However, since there is the same growth in E(t) for all three cases, the reduction in large scale growth for the initial structure simulations is accompanied by an amplification of small scale growth relative to the uniform field case. This is more prominent in the k8-16 case, as seen at t=2.5; the general shape towards small scales is the same however, with each case containing a local maximum near k/k_o=70. The initial structure for the k4-8 and k8-16 decreases slightly in peak energy as the spectra in each grows on small and large scales, and the peak smooths out. Due to the amplification of small scale fields relative to the uniform field case, the k4-8 and k8-16 simulations have regions where the magnetic energy is greater than the kinetic energy very early on. This region is larger in the k8-16 case, and can be seen already from t=0.2.

As the kinetic energy on the scales of the initial field structure and smaller grows, it serves to smooth out the initial peaks, causing a transfer of magnetic field energy to the smaller scales. It may be this feed down that suppresses the growth rate of the exponential phase of the small scale dynamo, as this effect is strongest near when the dynamo turns on in each simulation (near t=4.0). Since the field on the smallest scales is already well established in the initial field cases, it is already within an order of magnitude of the kinetic energy at small scales (and roughly a factor of five for the k8-16 case) when the dynamo becomes the dominant source of growth of the magnetic field. This is compared to nearly two orders of magnitude of separation for the uniform field case. This, combined with the dominance of the magnetic field over kinetic energy on medium scales, acts as a ceiling for the growth of the magnetic field. E_B growth rate then becomes limited by the E_K growth rate, contributing to the slower growth rate compared to the uniform case. From t$\sim$5 to t$\sim$10, the magnetic energy matches the kinetic energy for k$\geq$100. During this time, growth on the driving scale for k4-8 and k8-16 occurs at roughly the same rate as the uniform case, though the total energy on these scales is greater in the k4-8 simulation. At t=8.0, the spectra of the k4-8 and k8-16 simulations matches well for $k/k_o \geq$30.

Although the energy on the smallest scales was greatest for k8-16 in the early simulation, its growth rate diminishes significantly by t=9.0 here, as E_B for the k4-8 and uniform field cases quickly surpass it by t=10. Just before this, the uniform field is strongest near the driving scale and roughly matches

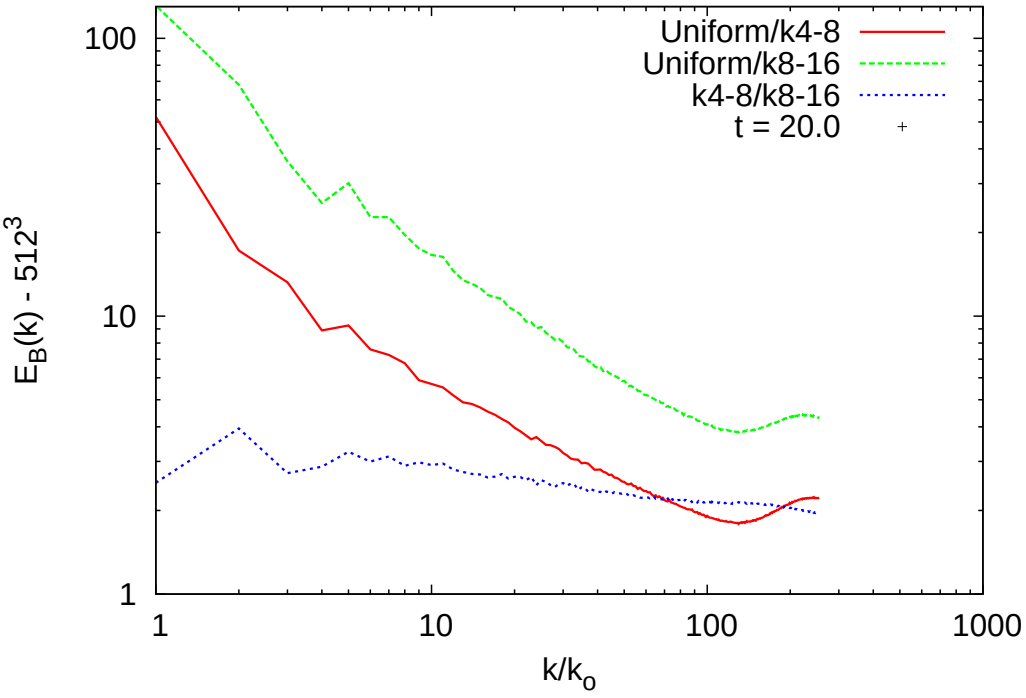

Figure 8: Shown is the ratio between the final (t=20) magnetic energy spectra for the uniform and k4-8 (red), uniform and k8-16 (green), and k4-8 and k8-16 (blue). The latter shows a nearly constant offset, while differences between k4-8 and k8-16 and the uniform field are significant on large scales and decrease towards small scales.

the other two simulations on the smallest scales. After t=10, the uniform field begins to enter the linear growth phase, growing past the kinetic energy on k>30, and growing with a flat spectrum towards the driving scale. Recalling Fig. 6, the linear growth phase is delayed for both the k4-8 and k8-16 cases. In this time, it appears the growth of E_B for the k4-8 simulation is still limited by growth rate of E_K on the smallest scales, struggling to surpass E_K on k/k_o >30 in the same fashion as the uniform field. This does eventually occur around t=18.5, at which point E_B does grow linearly. The k8-16 field evolution is further delayed compared to the other two cases, exhibiting a significant reduction in the growth rate of the exponential phase beginning around t=8.0. Throughout this reduction, the field remains completely below E_K, while, in contrast, k4-8 is able to surpass its E_K, even if for only a small region compared to the uniform field case. Although the k4-8 simulation is limited by E_K, it does match the kinetic energy growth rate; for k8-16 however, E_B is unable to keep up with the kinetic energy on the smallest scales, lagging behind throughout 8<t<16. By t=16, E_B growth for k8-16 better matches E_K, as the growth returns to the exponential form from t<8. Although k8-16 does not enter the linear growth phase by t=20 (the end of our simulations), the E_B spectra at t=20 is very similar to that of k4-8 at t=12. By this, I would conjecture that the k8-16 simulation will enter the linear growth phase near t=25.

By t=20, ignoring the obvious differences in power in total power, Fig. 8 the magnetic field spectra between the k4-8 and k8-16 simulations is roughly similar; however, the ratio is far from constant compared to the uniform case (there is a rough power law slope). Since the overall growth rate between the three simulations is different, the uniform field has more power over the entire spectrum than the k4-8 simulation, with the k8-16 simulation having the least. Near small scales, however, the differences between the three simulations decreases, though is still significant for the uniform case relative to the k8-16 case, primarily because the latter has yet to enter the linear growth phase in the small scale dynamo. Comparing the k4-8 and k8-16 cases, the former is greater by a roughly constant factor of $\sim$2.5, slightly higher near the driving scale, and slightly lower near the smallest scales. The main difference between the three simulations lies on the largest scale, near the driving scale. This is most pronounced comparing the two initial field structure simulations to the uniform case, where the uniform is greater than each at the driving scale by a factor of 40 and 105 for k4-8 and k8-16 respectively. It is apparent then, that the initial field structure plays a much larger role in modifying the characteristics of the magnetic field near the driving scale, rather than at the smallest scales. The small scale dynamo, then, does a fairly good job at establishing similar spectra at the smallest scales across all three initial field conditions.

The question remains as to what is different about the k4-8 and k8-16 evolution that would contribute to the additional suppression during the exponential growth phase, and the obvious differences in the small scale growth. The evolution of E_B and E_K spectra suggests that the relationship between each near the driving scale affects the nature of the growth between the three simulations. This is certainly true before the small scale dynamo becomes significant, but remains true throughout the entire simulation. When the uniform simulation makes the transition from exponential growth to linear growth, the magnetic field energy is within three orders of magnitude of the kinetic energy near the driving scale; at this same point, each of the two initial field structure simulations are around fiver orders of magnitude below E_K at the driving scale. It is not until E_B is within four orders of magnitude of E_K for k4-8 that there is significant growth above E_K on the smallest scales; this corresponds to the onset of the linear growth phase in this simulation. E_B for the k8-16 simulation remains greater than four orders of magnitude below E_K at the driving scale through t=20; this may be a significant contributing factor delaying the progress of the small scale dynamo, suppressing growth of E_B above E_K on the smallest scales. Again, the uniform field case does not have a problem making this transition because its magnetic field energy is already well established on large scales by t=8.0. It would seem that kinetic energy is cascading down faster than it is being fed into the magnetic field growth during the time small scale growth is surpassed. It is necessary to establish a significant large scale magnetic field for the small scale dynamo to operate effectively. We can conclude then that, although it is commonly thought that the field evolves as it is being fed upward from the smallest scales by the small scale dynamo, there is a significant component

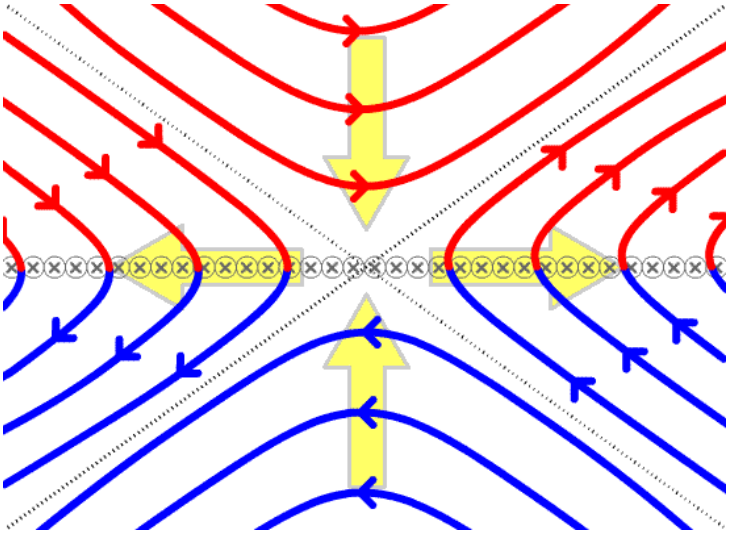

Figure 9: A cartoon picture showing a cross section of plasma undergoing magnetic reconnection. The absence of magnetic field in the center of the system is associated with a drop in pressure, pulling in plasma from the top and bottom. The opposing magnetic fields undergo reconnection, dissipating energy.

of field growth originating on the driving scale and feeding down to the smallest scales.

4.3 Isothermal Numerical Dissipation

Due to the presence of finite, but small, numerical resistivity in our simulations, it is possible for magnetic topologies to rearrange themselves to an equilibrium state through magnetic reconnection. This phenomena originates from the addition of a magnetic diffusion term ($\eta\nabla^2\vec{B}$) to the ideal induction equation, Eq. (3), in the non-ideal case. This term can be significant, even for cases of small electrical resistivity, in regions with large magnetic field gradients. Since current density $\vec{J}$ is correlated with large magnetic field gradients, as $\vec{J} = \nabla \times \vec{B}$, regions where this term becomes significant often form into physically large regions of high current density called current sheets. Even though magnetic field lines can be frozen in to the plasma in ideal MHD, the presence of a numerical resistivity allows for the rearranging of magnetic field lines locally around current sheets. It is through this rearranging that one would expect the dissipation of magnetic field energy in regions where the non-ideal induction term is significant.

The process that describes the dissipation of magnetic energy is illustrated in Fig. 9, and is referred to as magnetic reconnection. Regions like this form from large gradients in the magnetic field, and are located amidst current sheets. The ideal MHD limit does not allow for a proper description of what happens when fields in the plasma are arranged in this way; in true ideal MHD, there is no magnetic reconnection. Due to the large magnetic field gradient, the $\eta\nabla^2\vec{B}$ term in the non-ideal induction equation becomes significant, even for small resistivities. At the center of the region, there is no magnetic field,

causing a drop in the plasma pressure relative to its surroundings. Outside the central region, the ideal MHD limit still applies, and magnetic fields can be taken to be frozen into the plasma. Therefore, when the pressure drops and the surrounding plasma begins to fall into the center, the magnetic field lines come with it. However, once the opposing field lines meet, they rearrange themselves and reconnect, dissipating energy. This process repeats itself until the the newly formed field lines and plasma reach an equilibrium state, and the magnetic field gradient drops. The dissipation of the magnetic field energy is associated with an increase in the kinetic energy (from the infalling plasma), and thermal energy in the heating of the plasma. In adiabatic simulations, one could look for local temperature increases near where magnetic field energy is being dissipated, and associate them readily with magnetic reconnection. However, here we use an isothermal code, which does not conserve energy in cases such as this so as to maintain a fixed temperature. Any thermal energy that would be generated in a magnetic reconnection process is tossed out, or effectively "radiated away". True ideal MHD does not allow for magnetic reconnection or even dissipation in the first place, as magnetic topologies cannot be rearranged since they are frozen in to the plasma. However, in the case where there is a small but finite dissipation of magnetic energy, even in an ideal MHD context, non-ideal behaviors can occur. This is the situation here where, although we utilize an ideal MHD code with no explicit dissipation of magnetic energy, the presence of the numerical errors that arise from finite differences taken when solving the ideal MHD equations, cause the simulation to enter into the "weak limit" of non-ideal flows. These errors result in a small but finite numerical dissipation. By the exact conservation of mass, momentum, and magnetic flux in the code, it is hoped that the underlying physics is preserved, and the numerical dissipation functions physically. However, it is difficult to know whether the dissipation behaves physically, or if it is something else entirely. Finding the answer to the problem is made more complex since temperature is held constant, making finding and characterizing regions of numerical dissipation non-trivial.

As mentioned, dense current sheets form at the centers of regions undergoing a magnetic reconnection process. We begin by making a qualitative analysis of the presence of current sheets and the associated magnetic field lines. Fig. 10 shows a snapshot of a region of J^2 that is enhanced relative to the current in the surrounding plasma, the J^2 here his given by the color gradient shown at the bottom of each image. Since these samples were taken at around t=7, the peak current density is still low (purple) relative to the maximum (white) achieved in the simulations; all that matters here, however, is the relative intensity. The top left and top right images depict the same region viewed at the same orientation. The left contains just J^2, showing two adjacent current sheets, while the right contains J^2 with the inclusion of traces of magnetic field lines from a grid of sample points. As before, the color of the field lines, traveling from blue to white, denotes direction. As shown, the current density takes a form reminiscent of that seen in the magnetic reconnection images, with higher intensities located near large magnetic

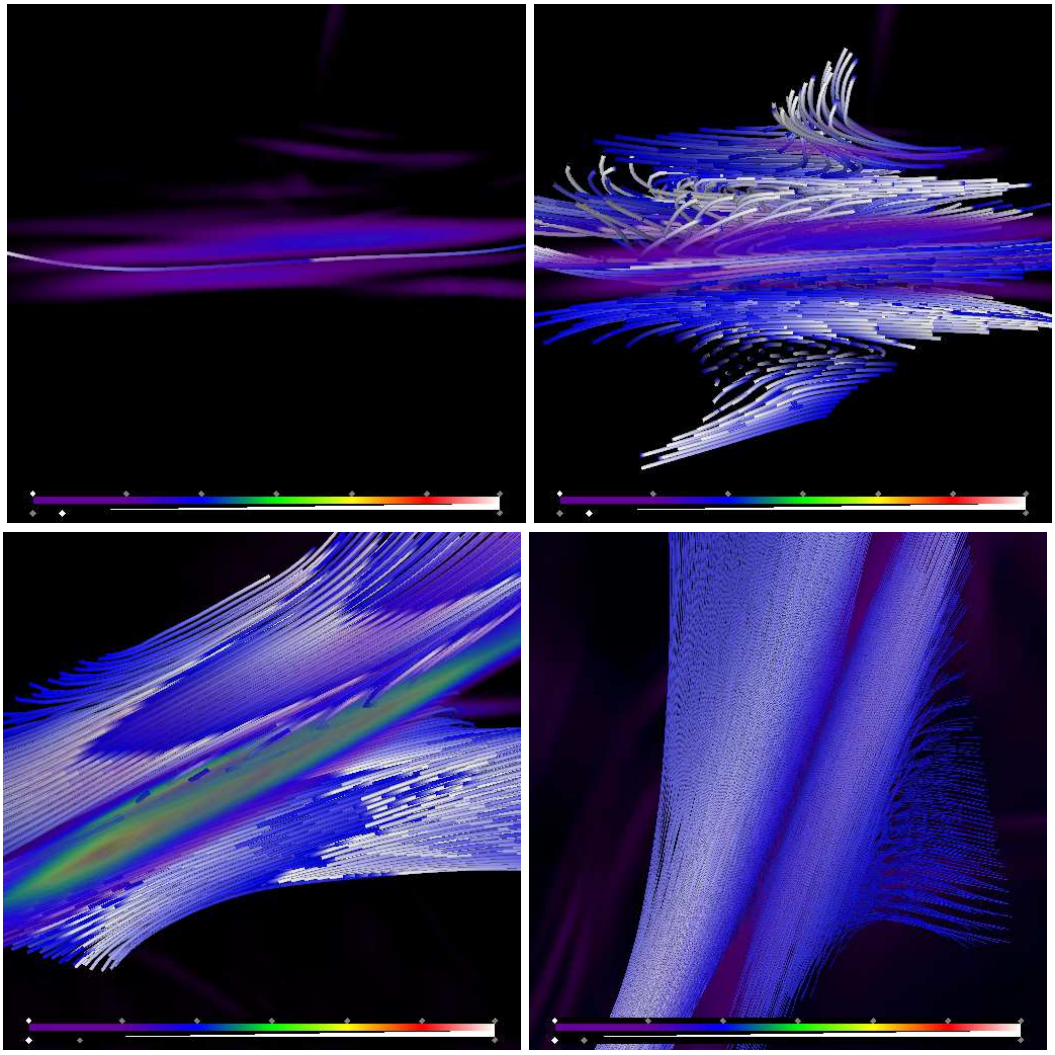

Figure 10: Shown is a volume rendering taken from the k4-8 512^3 simulation focused on a region of strong (relative to the surrounding area) J^2. The intensity of the current density in each panel is given by the color map at the bottom. The top left and top right images are the same view at the same time of the same two current sheets, shown in top left, with the top right image containing magnetic field line traces; again color (blue to white) traces direction along the field lines. The bottom two images are at separate locations and time in the simulation, and give just two other examples of similar cases as to that shown in the top two images.

field gradients, as denoted by the field lines that are tracing (generally) left to right just below the first current sheet, left to right in between the current sheets, and back to front right above the current sheet. The bottom two images are two separate examples of this same phenomena, taken at different times in the simulation, and at different locations (again time is irrelevant, as we are looking here at the regions of J^2 enhanced over the mean for the given time). The bottom left image shows a single current sheet with field lines traced above and below, traced left to right above, and right to left below. The bottom right image is similar as well, with the large current density existing in between the two dense packs of traced field lines; the field lines to the left of the current sheet seem to travel from the top of the image

down, while to the right of the sheet travel from the bottom of the image, up. A more quantitative look at what is seen here is explored below.

Although these images do not provide any concrete insight into the nature of the numerical dissipation in our simulations, they do grant a starting point for our examination. The observed relationship between current density and magnetic field motivates a comparison between J^2 and other simulation parameters. As mentioned previously, the ideal MHD induction equation excludes the dissipative term $\eta\nabla^2\vec{B}$. This term includes the effects of Ohmic dissipation and dissipation due to Maxwell stress forces. The induction equation can be used to readily write an equation for the time rate of change of the magnetic field energy given as

$$\frac{\partial E_B}{\partial t} = \vec{B} \cdot \left(\nabla \times \left(\vec{u} \times \vec{B} \right) + \eta \nabla^2 \vec{B} \right); \tag{5}$$

writing out the dissipative term into its components, this becomes

$$\frac{\partial E_B}{\partial t} = \vec{B} \cdot \left[\nabla \times \left(\vec{u} \times \vec{B} \right) + \eta |\vec{J}|^2 + \eta \nabla \left(\vec{J} \times \vec{B} \right) \right]. \tag{6}$$

Since the dissipation here is again numerical, the breakup of the dissipative term into its Ohmic and Maxwell stress terms is not justified as it would be in a non-ideal MHD case. However, we can construct a temporary proxy for the purposes of characterizing the the numerical dissipation. Since η is again numerical and poorly defined in all cases, we use $\vec{B} \cdot \nabla^2 \vec{B}$ as a means to identify possible regions where dissipation could occur in our simulations. Fig. 11 shows two examples of the promise of this comparison, giving an x-strip of J^2 (red) compared to $\vec{B} \cdot \nabla^2 \vec{B}$ (blue), with E_B shown in green; E_B is multiplied in each by a constant factor to more easily compare the three values. These are just but two examples of what is seen commonly throughout the simulation, in both other x-strips, and in the volume renderings like that shown in Fig. 10. In each image, two adjacent spikes of current density are are associated with an enhancement in the magnetic energy (note the different multiplicative factors on E_B between the two plots), and a sharp drop in the $\vec{B} \cdot \nabla^2 \vec{B}$ term, or, rather a sharp increase in the dissipation of magnetic energy at this location. This sharp increase in $\vec{B} \cdot \nabla^2 \vec{B}$ is a promising sign, but only gives dissipation at that location, and does not have an obvious relationship with the numerical diffusion we want to explore. The goal here would be to develop a means to connect the observed dissipation of magnetic energy to actual numerical diffusion in a reliable way, and then characterize this new quantity. These results just barely scratch the surface as to characterizing the numerical dissipation, but provide some important insight into the matter. We will discuss possible next steps in this analysis in Sec. 6.

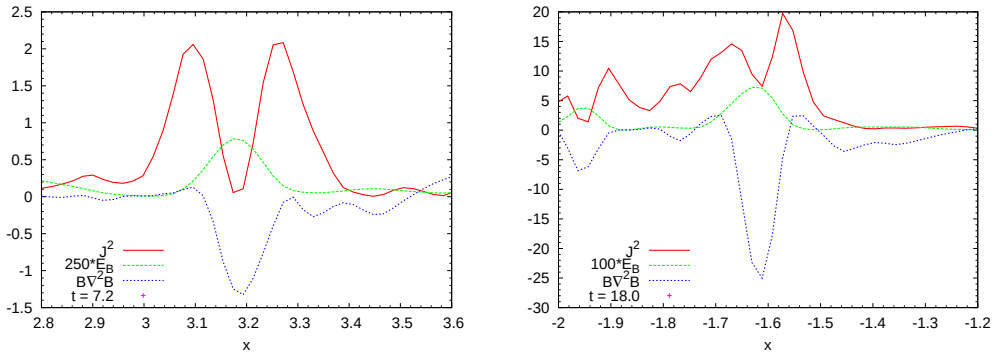

Figure 11: Shown is a comparison of J^2 (red), $\vec{B} \cdot \vec{\nabla}^2 \vec{B}$ (blue), and E_B (green) at two different locations at two different times, t=7.2 (left), and t=18.0 (right) for an x-strip of the simulation volume. E_B is multiplied by a constant factor to better compare to the other two values.

5 Discussion

Based upon the examination of E(t) and E(k) for both the magnetic field and velocity field, it is apparent that the small scale turbulent dynamo, though a fairly good descriptor of the interplay between turbulence and magnetic fields, is not the complete picture of what is a complex process. There is significant divergences from the simple picture given by the dynamo that manifest themselves as a function of initial magnetic field structure. In the case of the uniform magnetic field, the examination of E(t) shows that, once the dynamo turns on, the field grows as expected, entering an exponential growth phase, followed by a linear growth phase. However, it is apparent that the onset of these stages is a function of the initial conditions on the magnetic field, in that the conditions presented here delay the point with which magnetic backreaction becomes significant. In addition, the initial conditions modify the character of the growth rate during the exponential stage. As determined by examining E(k), it is the case that there is a significant difference in growth rates of E_B near the driving scale between the three simulations.

For the evolution before the onset of the small scale turbulent dynamo, we observe that the resulting E(t) is characteristically the same in all three cases, with divergences beginning to occur only when the small scale turbulent dynamo begins to turn on in the three simulations. In this time, growth on scales nearest the driving scale is dominant, with the total power supplied to E_B here being comparable in all three initial field cases. The velocity field then appears to be very efficient at feeding into the magnetic field energy near the driving scale, regardless of initial field conditions. The actual spectra in these wave numbers appears shifted depending upon initial conditions, but, again, the total power delivered by the driven plasma remains similar. Because of this, and because of the overall shift of the magnetic spectra in wave number for each simulation near the onset of the small scale turbulent dynamo, the larger presence of E_B on small scales for k8-16 and k4-8 inhibits the growth rate of E_B substantially.

Since the uniform case remains uninhibited, relative to the other two field cases, it is able to grow quickly to the linear growth phase without resistance. The reason for the suppressed slopes of k4-8 and k8-16 in the exponential phase (especially for the latter, with the dip halfway through), appears to be a pile up of energy on the smallest scales, which is inefficiency transferred to E_B.

In spite of the fact that the effect of the small scale turbulent dynamo on each simulation is characteristically different, each simulation begins to converge to a similar spectra by the timescale of just over one large eddy turnover time. The magnetic field spectra is different near the driving scales for each simulation, especially relative to the uniform case, but there is mostly only a difference in power between k4-8 and k8-16. These differences will themselves be erased as the plasma approaches the final saturation state at large t. There is a finite window of time then that there are significant, possibly identifiable, differences between magnetic field spectra as a result of the initial magnetic field structures. Although we focus on three initial magnetic field conditions, this is by far not an exhaustive exploration into all possible initial field cases. In galaxy clusters, the most significant injection of magnetic flux occurs in major merger events, as turbulence is generated through shocks and infalling plasma. The timescales with which this process occurs is not currently identifiable through observation, but can be explored through cosmological cluster formation simulations.

Paul et al. (2011) presents the results of cosmological scale simulations studying the effects of major mergers in galaxy clusters on shock and turbulence development; we reference this work in order to extrapolate our simulations to a galaxy cluster context. As show in Fig. 11 from Paul et al. (2011), the pressure support from the developed turbulence reaches a maximum of around 1/2 the total thermal pressure. The simulated clusters, much like real clusters, reach temperatures on the order of 10^7 K on average, and up to 10^8 K in cluster centers. We take T$\sim$5 keV ($\sim 6\times10^7$K) as a characteristic temperature for the turbulent regions of these clusters (i.e. near shocks). Taking $P_{turb}=u_{RMS}/3$ and $P_T=kT/\mu m_p$, where μ=0.6 amu is the mean molecular weight, m_p is the proton mass, and k is Boltzman's constant, one can calculate a characteristic sound speed within the turbulent regions of $\sim$1100 km/s, or 1.1 kpc/Myr. Although the turbulent driving scale is not known exactly in a cluster context, we would expect them to be some fraction of the scales of shock curvature radii and of cluster substructures, such as an active galaxy or galactic outflows; this means eddies should exist on scales of a few 10s to a few hundred kpc. In the case of shocks, we can pick a typical range of driving scales as 100-200 kpc. The corresponding eddie turnover time at these scales ($t_o=L_d/u_{RMS}$) would then be on the order of a few Myr, or 100-200 Myr. The decay time for the turbulence generated in these simulations, and therefore the time during which the magnetic field would be evolving, is on the order of 1 Gyr in the case where $P_{turb}/P_{therm}=1/2$. By these estimates, then, we would expect that the ICM in a galaxy cluster experiences anywhere from a few to around 10 eddy turnover times during major merger events.

The corresponding eddy turnover time in our simulation is around 10 time units. Examining E(t) in Fig. 6, our simulations go out to t=20, or roughly two eddy turnover times. The relevant time, looking at E(k) in Fig. 7, during which the magnetic fields are distinguishable is $\lesssim$1 eddy turnover time. Thus, by these estimations, we would expect that a significant amount of information about initial field structures is lost within the first few Myr of turbulence generation from a major merger. Therefore, we would expect that some information of the initial structure of galaxy cluster magnetic fields could be extracted from observation if one could find a galaxy cluster that has, within a few Myr of observation, undergone a major merger event. Faraday rotation measurements would be the best means to identify the structure of the magnetic field in galaxy cluster ICM. However, it is an issue as to whether or not the magnetic field structures would be resolvable to a degree necessary to be able to glean information from the field initial states. Doing so would require an observation of a large volume of the galaxy cluster's ICM, in order to develop a three dimensional picture of the field structure, as opposed to just a line of sight projection. This must be done at high resolution over a very large range of wavelengths. Beck et al. (2012) gives a detailed overview of what would be possible in this context using measurements made with both current radio telescopes and the upcoming Square Kilometer Array (SKA); Stepanov et al. (2008) gives a more detailed analysis of the possible science output of the SKA alone. From their models, it would be theoretically possible to synthesize data from several current radio telescopes, such as LOFAR, WRST, GMRT, and the EVLA, to provide a large enough range of wavelegnths to be able to identify magnetic field structures on small, intermediate, and large scales. However, constructing such a synthesis is non-trivial, and would still be limited when compared to what would be possible with the SKA. The SKA would, by its first phase, expected in 2019, be able to make high resolution observations over the entire wavelength range covered by the synthesis of current telescopes, corresponding to a frequency range of 70 MHz to 10 GHz. These potential new observations of magnetic field structures in the ICM, utilized in harmony with additional simulation work of magnetic field structures in plasmas and clusters, would provide unprecedented insight into how magnetic fields evolve in clusters, and, in some cases, their origin.

6 Conclusion

Magnetic fields play an essential role in almost all astrophysical objects. In the case of the intracluster medium, these fields are observed to be present with a strength on the order of $\sim 0.1\mu$G. They are thought to play a significant role in governing properties of the ICM, including its viscosity, resistivity, and thermal conductivity, and are thought to contribute in part to the injection of energy into the synchrotron emission that is seen in cluster radio halos. The weather of the ICM serves as a mechanism

to generate turbulence within the ICM, which in turn amplifies and evolves an originally week seed field to the levels seen in observation. In this paper, we examined the detailed interplay between this turbulence and an already established weak magnetic field in order to better extract information that could better explain the relationship between these two in the situation of ideal, isothermal MHD. It is expected that the small scale turbulent dynamo is the most significant mechanism by which these fields evolve, and governs E_B(t) in three distinct stages: 1) exponential growth, 2) linear growth, and 3) a saturation stage. At very early times in this process, the exact details of field evolution are not yet well understood. We construct a few different simulations, varying the initial conditions on the magnetic field and observing its evolution at very early times.

In this analysis, with results given in Sec. 4, and their discussion in Sec. 5, we outline the major results:

1. The small scale dynamo is seen to play an important role in the evolution of each initial magnetic field case, but does not completely describe the evolution of E_B(t) or E_B(k). Its ability to describe the field evolution is dependent upon the initial conditions of the magnetic field. In addition, evolution of E_B on the driving scale is significant, especially for early times, and even after the small scale dynamo turns on. The establishment of large scale E_B is necessary for continued growth on small scales.

2. Regardless of initial field condition, we see that, with a possible difference in total final power, the initial conditions produce very similar final (t=20) spectra, especially when comparing the two cases with structure to the initial field. This could be significant for observation, as a young enough cluster, early in the merging process perhaps, could still show some remnants of its initial field structure a few Myr after a merger event. With significant synthesis work using current telescopes, or studies with future radio telescopes, observations of detailed magnetic field structure in clusters is possible, and, depending on the dynamics of the cluster, could provide insight into the initial field structure.

The results of this paper can be expanded upon in several ways. The first is by extending this analysis to higher resolution simulations than those presented here. It is important when conducting computational simulations of real systems to perform sanity checks to assure the validity of the results (i.e. that the results are physical). This is performed rigorously for our numerical methods in the references outlined in Sec. 2, but can be tested on a simulation by simulation basis by observing the convergence of the results as one increases resolution. Choosing an arbitrarily large resolution from the start of a given analysis is prohibitively expensive, which is why simulations are often performed at very low resolution, and increased progressively until the convergence is satisfactory, or until one is

limited by resources. Depending on the complexity of the initial conditions and the properties of a given simulation, a varying resolution may be required to be confident that one is not missing key information by remaining at a given resolution. For example, it is likely that the hydrodynamical simulation, with no magnetic field, would require a lower resolution to be sufficiently convergent. In order to check the results presented in this paper, one would reproduce this analysis at 1024^3 resolution. This next step is already in the progress for one of the above simulations (k4-8). A preliminary analysis shows that, although there are definite quantitative differences, there is nothing qualitatively different of significance between the 512^3 resolution presented here, and the 1024^3 resolution. This is expected to be the case as well for k8-16 and the uniform field, but performing the higher resolution simulation is still necessary.

With regards to the dissipation analysis, there is still a significant body of work that could be performed on the identified regions of interest. We have already begun a preliminary analysis to attempt to quantify and extract exactly the numerical dissipation occurring in a given localized region of the plasma box, trying to understand its relationship to E_B, J^2, $\vec{B} \cdot \vec{\nabla}^2 \vec{B}$, and etc. The objective is to isolate the Ohmic dissipation component of this quantity, if it exists, and determine whether or not the numerical dissipation truly behaves like physical processes, like reconnection, or if it is something else entirely.

Finally, as discussed previously, we examine only a small dynamical range of the total problem of understanding the ICM specifically, and the relationship between turbulence and magnetic fields in astrophysical plasmas in general. Although it is ultimately a matter of computational resources that limits the simulation of the entire situation in galaxy clusters, from the largest eddies down to the dissipative and resistive scales, one could see a possible avenue for improvement of this analysis by extending what we have demonstrated in ideal, isothermal MHD to non-ideal MHD. A proper treatment of the detailed microphysics seen in the ICM would require the non-trivial but possible inclusion of explicit viscous and resistive dissipation terms as corrections to the ideal MHD code utilized here. With the inclusion of resistive dissipation, the magnetic field would now depend also on the electric field present in the plasma, requiring additional modification to the numerical scheme. However, doing this would allow the inclusion of an explicit physical magnetic dissipation, and reveal in more detail the exact relationship between the generated turbulence and growth of the magnetic field. Repeating this analysis with non-ideal MHD is likely to provide a better insight into the physical situation in the ICM.

7 Acknowledgments

A.E was supported in part through the University of Minnesota Undergraduate Research Opportunities Program grant. I would like to thank Dr. Tom Jones and Dr. David Porter for their roles in advising

on this project, and for remaining patient with me from the beginning through the end. In addition, I would like to thank them and Dr. Lawrence Rudnick for being willing to read the final edition of this thesis, and for their valuable input with its first drafts.

References

Beck, R., Frick, P., Stepanov, R., & Sokoloff, D. 2012, , 543, A113

Brandenburg, A., & Subramanian, K. 2005, , 417, 1

Brunetti, G., Setti, G., Feretti, L., & Giovannini, G. 2001, , 320, 365

Carilli, C. L., & Taylor, G. B. 2002, , 40, 319

Cho, J., Lazarian, A., & Vishniac, E. T. 2002, , 564, 291

Cho, J., & Yoo, H. 2012, , 759, 91

Evans, C. R., & Hawley, J. F. 1988, , 332, 659

Harten, A. 1983, Journal of Computational Physics, 49, 357

Kang, H., Ryu, D., Cen, R., & Ostriker, J. P. 2007, , 669, 729

Kim, J., Ryu, D., Jones, T. W., & Hong, S. S. 1999, , 514, 506

Medvedev, M. V., Silva, L. O., & Kamionkowski, M. 2006, , 642, L1

Paul, S., Iapichino, L., Miniati, F., Bagchi, J., & Mannheim, K. 2011, , 726, 17

Roe, P. L. 1981, Journal of Computational Physics, 43, 357

Ryu, D., & Jones, T. W. 1995, , 442, 228

Ryu, D., Jones, T. W., & Frank, A. 1995, , 452, 785

Ryu, D., Kang, H., Cho, J., & Das, S. 2008, Science, 320, 909

Ryu, D., Kang, H., Hallman, E., & Jones, T. W. 2003, , 593, 599

Ryu, D., Miniati, F., Jones, T. W., & Frank, A. 1998, , 509, 244

Ryu, D., Schleicher, D. R. G., Treumann, R. A., Tsagas, C. G., & Widrow, L. M. 2012, , 166, 1

Schekochihin, A. A., Cowley, S. C., Taylor, S. F., Maron, J. L., & McWilliams, J. C. 2004, , 612, 276

Skillman, S. W., O'Shea, B. W., Hallman, E. J., Burns, J. O., & Norman, M. L. 2008, , 689, 1063

Stepanov, R., Arshakian, T. G., Beck, R., Frick, P., & Krause, M. 2008, , 480, 45

Strang, G. 1968, SIAM Journal on Numerical Analysis, 5, 506

Takami, H., Inoue, S., & Yamamoto, T. 2012, Astroparticle Physics, 35, 767